

# A modulated nonlinear system: breathers and time crystals

Masayuki Kimura,<sup>1</sup> Juan F. R. Archilla,<sup>2, a)</sup> Yusuke Doi,<sup>3</sup> and Víctor J. Sánchez-Morcillo<sup>4</sup>

<sup>1)</sup>Department of Electrical and Electronic Engineering, Faculty of Science and Engineering  
Setsunan University, 17-8 Ikeda-Nakamachi, Neyagawa, Osaka 572-8508, Japan

<sup>2)</sup>Grupo de Física No Lineal, Universidad de Sevilla, ETSI Informática, Avda Reina Mercedes s/n, 41012-Sevilla, Spain

<sup>3)</sup>Division of Mechanical Engineering, Graduate School of Engineering, The University of Osaka, 2-1 Yamadaoka, Suite, Osaka 565-0871, Japan

<sup>4)</sup>Universitat Politècnica de València, Instituto de Investigación para la Gestión Integrada de Zonas Costeras (IGIC), Paranimf 1, 46730 Grao de Gandia, València, Spain

In this work we study space-time modulated system using as a specific example a system of cantilevers with their on-site potential provided by electromagnets fed with DC and AC currents. The system equations are deduced and the effect of the modulation on the dispersion bands is examined. We adapt the theory of breather existence and stability to space-time modulation. We concentrate the numerical calculations in time-modulated system for which we have obtained different types of breathers for a wide range of frequencies that can be classified in two different classes (i) the modulation frequency is an integer multiple of the breather frequency and (ii) the breather frequency is an integer multiple of the modulation frequency. The first class, corresponds to the formation of time crystals as there is no entropy production. The construction of a similar system would be of interest to study the properties of dynamic metamaterials.

PACS numbers: 63.20.Pw, 63.20.Ry, 05.45.-a, 02.70.-c

Keywords: nonlinear waves, breathers, thermal equilibrium, localization, intrinsic localized modes (ILM)

## I. INTRODUCTION

Arrays of coupled cantilevers have been constructed and modeled to study nonlinear vibrations<sup>1</sup>, because they are relatively simple to build, they are macroscopic and can be driven by different types of forces. In particular, localized, periodic vibrations called intrinsically localized modes (ILM) or discrete breathers (DB)<sup>2</sup> appear in these systems. ILMs may have different patterns; the simplest one is the Sievers-Takeno (ST) mode, where a single oscillator, called the center, has an amplitude much larger than its nearest neighbors, so the amplitude decreases rapidly with the distance to the center. In this state, all the oscillators vibrate in phase, with a frequency smaller than the isolated oscillators. The ST mode exists and is stable if the on-site potentials are soft, that is if their frequency increases with the distance. Other mode is the Page (P) mode<sup>3,4</sup>, where two neighboring oscillators have the same amplitude, being therefore a double ILM or breather. The P-mode is stable for hard potentials and has a frequency above the phonon band<sup>5</sup>.

An array of cantilevers was also presented in Ref. <sup>6</sup>. The system was driven by a periodic force applied to the support of the cantilevers, appearing as an independent external force in the dynamical equations. The restoring force had two contributions: one provided by the elastic properties of the cantilever, and other of magnetic nature, by fixing a magnet at the free end of the cantilever, and locating an electromagnet below it. The magnetic force due to permanent magnet-electromagnet interaction, can be tuned by changing an electric DC current,

in this way, a tunable on-site potential is obtained. The system resulted in breathers having different properties depending on the current magnitude and the frequency. These and similar models have been used in the study of ILMs<sup>7-11</sup>.

In this paper we present a variation of the model introduced in Ref. <sup>6</sup>, but incorporating, besides the static (DC) current, an oscillating (AC) contribution in the electromagnets. This bring about an on-site potential that it is tunable and periodic in time. Furthermore, introducing phase differences between neighboring cantilevers, an on-site potential with a space-time modulation is achieved. An experimental and mathematical model with a linear on-site potential and nonlinear coupling has been studied<sup>12</sup>, finding  $q$ -gap breathers. In our case the on-site potential is nonlinear and the coupling is linear.

The article is organized as follows: after the introduction in Sect. I, Sect. II presents the physical model and the derivation of the system of differential equations both for the nonlinear system and its linear approximation corresponding to small oscillations. In Sect. III, the effect of space and time modulation on the dispersion bands is analyzed theoretically and numerically. Sect. IV presents changes brought about by modulation in breather theory, breather obtention, and stability. In Sect. V, time-crystal breathers, that is, breathers with a frequency an integer multiple of the modulation frequency, are obtained and their properties presented. The case of the breather frequency as a multiple of the modulating frequency is presented in Sect. VI. The final Sect. VII presents the concluding remarks.

<sup>a)</sup>Corresponding author: archilla@us.es

## II. PHYSICAL SYSTEM AND DYNAMICAL EQUATIONS

In this section we derive from physical laws the dynamical equations. A sketch of the physical model is shown in Fig. 1.

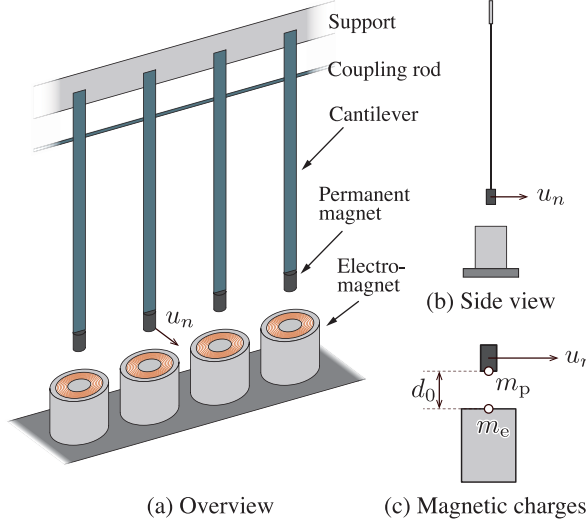


FIG. 1. System of cantilevers mechanically coupled by a rod. (b) Side view of a cantilever. A permanent magnet is attached at the tip of the cantilever. An electromagnet is placed below the permanent magnet. (c) Definition of magnetic charges. Modified with permission from Ref. <sup>6</sup>

The variable  $u_n$  measures the horizontal deviation of the cantilever tip with respect to its equilibrium position. The vertical distance between the electromagnet and the cantilever tip is  $y_n$ , therefore, the position vector of the tip with respect to the electromagnet is  $\vec{r}_n = u_n \hat{e}_x + y_n \hat{e}_y$ , with equilibrium position  $\vec{r}_{n,0} = d_0 \hat{e}_y$ , and modulus  $r_n = \sqrt{u_n^2 + y_n^2}$ . Within the formulation of magnetic charges, analogous to the Coulomb law, the magnetic force is given by  $\vec{F}(\vec{r}_n) = \frac{1}{4\pi\mu_0} \frac{m_p m_e}{r_n^2} \hat{r}_n$ <sup>13</sup> with  $m_p$  and  $m_e$  the magnetic charges of the permanent magnet and the electromagnet, respectively, and  $\hat{r}_n$  the unitary vector in the direction of  $\vec{r}_n$ . Assuming small cantilever angles,  $y_n \simeq d_0$  and the horizontal force component per unit mass becomes

$$F(u_n) = \frac{m_p m_e}{4\pi\mu_0 M} \frac{u_n}{(u_n^2 + d_0^2)^{3/2}}. \quad (1)$$

The force must obviously depend on the current  $I_{EM}$  of the electromagnet. The first factor in Eq.(1) can be identified with an interaction coefficient (per unit mass,  $\chi(I_{EM})$ ), which may be alternatively expressed as a function of the driving current  $I_{EM}$  as  $\chi(I_{EM}) = \chi_0 + \chi_1 I_{EM}$ . The constant term  $\chi_0$  in the interaction coefficient is due to the ferromagnetic core of the electromagnet, while the variable term  $\chi_1$  is due to the magnetic field created by

the current of the electromagnet. Note that  $\chi_0 < 0$ , corresponding to the attraction of the ferromagnet and  $\chi_1$  depends on the polarity of the current, which is such that in this work  $\chi_1$  is also negative. The current consists of a DC and a modulated AC components, i.e.,

$$I_{EM}(n, t) = I_{DC} + I_{AC} \cos(hn - \Omega t) \quad (2)$$

Therefore the dynamical equations become:

$$\ddot{u}_n = -\omega_{0,0}^2 u_n + F(u_n) + C(u_{n+1} + u_{n-1} - 2u_n) \quad (3)$$

where  $\omega_{0,0}$  is the natural frequency of an isolated cantilever,  $C$  is the coupling constant, and the force is given by

$$F(u_n) = -(|\chi_0| + |\chi_1| I_{EM}(n, t)) \frac{u_n}{(u_n^2 + d_0^2)^{3/2}} \quad (4)$$

Typical values of the parameters for the cantilever system, obtained in a previous experiment, are  $\omega_{0,0} = 2\pi \times 35.72 \text{ rad/s}$ ,  $d_0 = 3 \text{ mm}$ ,  $\chi_0 = -4.71 \times 10^{-5} \text{ m}^3 \text{s}^{-2}$ ,  $\chi_1 = -9.14 \times 10^{-3} \text{ m}^3 \text{s}^{-2} \text{ A}^{-1}$  and  $C = 284 \text{ s}^{-2}$ .

Expanding the last term in Eq.(4), results in

$$\frac{u_n}{(u_n^2 + d_0^2)^{3/2}} = \frac{u_n}{d_0^3} - \frac{3}{2} \frac{u_n^3}{d_0^5} + o(u_n^5) \quad (5)$$

evidencing that the on-site potential is of soft type. Keeping only the linear term we obtain the linearized equations:

$$\begin{aligned} \ddot{u}_n = & -\omega_{0,0}^2 u_n \\ & - \left( \frac{|\chi_0| + |\chi_1| I_{DC}}{d_0^3} + \frac{|\chi_1| I_{AC}}{d_0^3} \cos(hn - \Omega t) \right) u_n \\ & + C(u_{n+1} + u_{n-1} - 2u_n), \end{aligned} \quad (6)$$

The frequency of small oscillations of a non-modulated isolated oscillator is, therefore,  $\omega_{0,\text{phys}} = (\omega_{0,0}^2 + |\chi_0| + |\chi_1| I_{DC})^{1/2}$ .

$$\ddot{u}_n = -\omega_0^2 u_n - \delta \cos(hn - \Omega t) u_n + \kappa(u_{n+1} + u_{n-1} - 2u_n), \quad (7)$$

with  $\omega_0 = 1$ , that we keep for clarity,  $\kappa = C/\omega_{0,\text{phys}}^2$ , and  $\delta = \frac{|\chi_1| I_{AC}}{\omega_{0,\text{phys}}^2 d_0^3}$ .

The non-linearized model, in the scaled variables, results

$$\begin{aligned} \ddot{u}_n = & -\omega_0^2 u_n \\ & - \omega_0^2 \left( -\frac{1}{d_0^3} u_n + (1 + \delta d_0^3 \cos(hn - \Omega t)) \frac{u_n}{(u_n^2 + d_0^2)^{3/2}} \right) \\ & + \kappa(u_{n+1} + u_{n-1} - 2u_n), \end{aligned} \quad (8)$$

for  $\bar{d}_0 = d_0/\sigma$ . The second term multiplied by  $\omega_0^2 = 1$  is written in that way because it is completely nonlinear

when expanding the terms in  $u_n$ . It also highlights that the linear frequency of the unmodulated system of the isolated oscillator is  $\omega_0 = 1$ .

The nonlinear equations in a more condensed form are:

$$\begin{aligned} \ddot{u}_n &= -\omega_0^2 u_n \\ &- \omega_0^2 \left( -\delta_1 u_n + (1 + \delta_2 \cos(hn - \Omega t)) \frac{u_n}{(u_n^2 + \bar{d}_0^2)^{3/2}} \right) \\ &+ \kappa(u_{n+1} + u_{n-1} - 2u_n), \end{aligned} \quad (9)$$

with  $\delta_1 = 1/\bar{d}_0^3$  and  $\delta_2 = \delta \bar{d}_0^3$ .

For a representative set of parameters of currents, we fix DC and AC amplitudes as  $I_{AC} = I_{DC} = 12$  mA, and in order to obtain that  $\omega_0 = 1$ , the scaling factors are  $\tau = 4.286$  ms and  $\sigma = 1.423$  mm, leading to  $\bar{d}_0 = 2.1087$ ,  $\kappa = 0.0051632$ ,  $\delta_1 = 0.10665$ ,  $\delta_2 = 0.6996$ .

The linearization of (9) leads again to the system (7), with  $\delta = \delta_2/\bar{d}_0^3 = \delta_2 \delta_1 = 0.07461$  for the chosen currents.

In the following we will write  $d_0$  instead of  $\bar{d}_0$  for simplicity.

### III. EFFECT OF SPACE-TIME MODULATION ON THE LINEAR DISPERSION

In this section we consider the linear system described above in (7) which is valid for small displacements  $u_n$ .

For  $\delta = 0$ , the system is a well known, Klein-Gordon system, having a basis of solutions  $\exp(iqn - \omega t)$ , with  $\omega_q^2 = \omega_0^2 + 4\kappa \sin^2(q/2)$ . Note that for a given  $q$  there are two frequencies  $\pm\omega$  that are also frequencies for  $-q$ .

For a finite system with  $N$  units and periodic boundary conditions the possible values of  $q$  are  $q_m = 2\pi m/N$ , with  $m = 0, \dots, N-1$ , this includes also negative values of the wavevector  $q = -q'$ , with  $q' > 0$ , as any wave number  $q$  is equivalent to  $q \pm 2\pi n$ . Also, any set of numbers  $m' = m + n$ , where  $n$  is any integer lead to an equivalent basis, a convenient one, centered around  $q = 0$  is  $-N/2, \dots, N/2 - 1$  if  $N$  is even or  $-(N-1)/2, \dots, (N-1)/2$  if  $N$  is odd. An alternative basis in real space is given by  $\cos(qn - \omega t)$  and  $\sin(qn - \omega t)$ , but the exponential basis functions are more convenient analytically.

We first describe the effect of introducing the modulation term with  $\delta > 0$  small as observed in numerical simulations. Then we will obtain approximately the new dispersion relations, for several cases and the general case.

Using initial uniformly random conditions for  $u_n$  and letting the system evolve to thermal equilibrium and performing the 2D fast Fourier transform (2DFFT) we obtain the energy density plot and the  $\omega - q$  spectrum shown in Fig. 2 :

We can see that new dispersion bands appear roughly parallel to the unmodulated one and with their maxima and minima displaced.

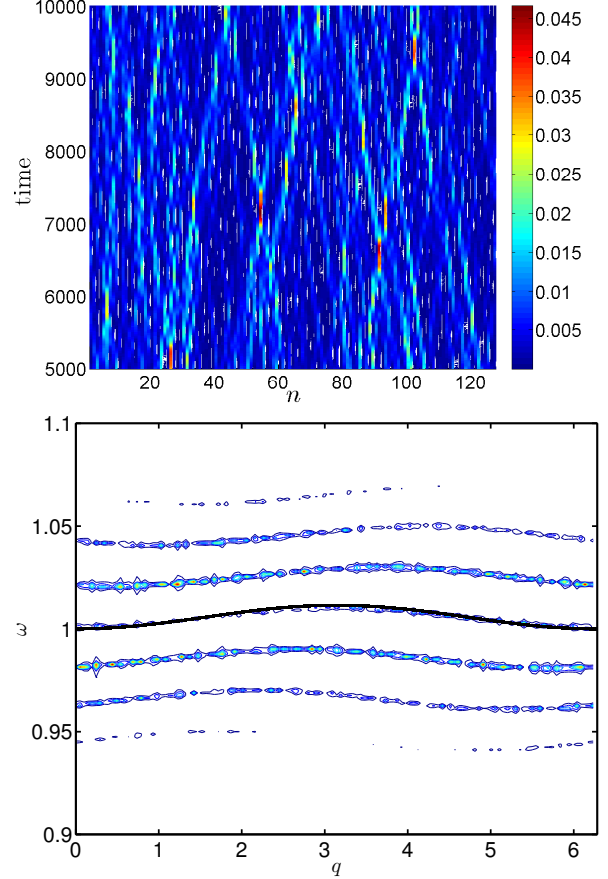


FIG. 2. Numerical simulations after thermalization with modulation frequency and wave number  $\Omega = 0.02$  and  $h = 0.5$  : (Top:) Energy density plot (Bottom) 2D FFT.

#### III.A. Dispersion bands modification with only space modulation

In order to understand the result we will consider first the case  $h = 2\pi/L$ , where  $L$  is an integer, and  $\Omega = 0$ . In this case, the symmetry of the system  $n \rightarrow n + 1$  is broken and substituted by the symmetry  $n \rightarrow n + L$ . Let us suppose that  $\delta = 0$ , but still the symmetry is broken, then, in order to be able to impose periodic boundary conditions, we need that  $N = RL$  with  $R$  and integer number. Now, by Bloch theorem<sup>14</sup>, the solutions are of the form  $\exp(iqn)F(n, t)$ , with  $F(n, t)$  a solution with the periodicity of the lattice, whose period is now  $L$ , that is the elements of the basis are given by  $u_{l,r} = \exp(iqn) \exp[i(qn - \omega t)]$ . As the second factor has the periodicity of the new lattice  $q_l = (2\pi/L)l$ , with  $l = 0, \dots, L-1$ . If we impose periodic boundary conditions, then  $u_{l,r}(n, t) = u_{l,r}(n + N, t)$ , the second factor is automatically identical if  $N = RL$  and the first factor becomes  $q_r = 2\pi r/N$ , with  $r = 0, \dots, R-1$ , as larger values of  $r$  can be written as  $q'_r = 2\pi(r_1R + r_2)/N = 2\pi(r_1R + r_2)/LR = 2\pi r_1/L + 2\pi r_2/N$ , and the first term

is periodic in  $L$  and can be incorporated into  $F(n, t)$ . We can rewrite it as:

$$\begin{aligned} u_{n,t} &= \exp(iq_l n) \exp(iq_r n) \exp(-i\omega_{l,r} t) \\ &= \exp(i\frac{2\pi r}{N} n) \exp(i\frac{2\pi l}{L} n) \exp(-i\omega_{l,r} t), \end{aligned} \quad (10)$$

with  $r = 0, \dots, R-1$  and  $l = 0 \dots L-1$ . The original index  $m = 0, \dots, N-1$  is given by  $m = rL + l$ , and the frequencies are given by

$$\omega_{l,r}^2 = \omega_0^2 + 2\kappa(1 - \cos(\frac{2\pi l}{L} + \frac{2\pi r}{N})). \quad (11)$$

In the following, we use the standard notation of ket and bras summarized in Appendix A.

The solutions of the system  $H_0|u\rangle = E_0|u\rangle$ , with  $E = \omega^2$  are given by the eigenvectors of  $H_0$  with the same eigenvalue  $E = \omega^2$ . There are two eigenvectors with the same eigenvalue, corresponding to  $|k\rangle$  and  $|-k\rangle$ , the latter being equivalent to  $|N-k\rangle$  under periodic boundary conditions. Their eigenvalues are  $E_0 = \omega^2 = \omega_0^2 + 2\kappa(1 - \cos(\frac{2\pi k}{N}))$ .

The solution to the eigenvalue equation of the perturbed Hamiltonian

$$(H_0 + \delta H_1)|\phi\rangle = (E_0 + \delta E_1)|\phi\rangle$$

will be in the first approximation close to the eigenspace of  $E_0$ , that is some linear combination of  $|k_1\rangle \equiv |k\rangle$  and  $|k_2\rangle \equiv |-k\rangle$  (it can be done with the cosine and sine solutions but the theory has to be reformulated and does not add any value). So, let us suppose that  $|\phi_1\rangle$  is a linear combination of the orthogonal eigenvectors, i.e.,  $|\phi_1\rangle = \alpha|k_1\rangle + \beta|k_2\rangle$  and then, we obtain

$$E_0|\phi\rangle = H_0|\phi\rangle \quad \text{and} \quad E_1|\phi\rangle = H_1|\phi\rangle,$$

and we can write  $|\phi\rangle = |\phi_1\rangle$ . The first equation holds because  $\phi$  is in the  $E_0$ -eigenspace of  $H_0$ . Substituting  $|\phi_1\rangle$  and using that  $H_1$  is linear, we obtain:

$$E_1(\alpha|k_1\rangle + \beta|k_2\rangle) = \alpha H_1|k_1\rangle + \beta H_1|k_2\rangle.$$

Multiplying by the left by  $\langle k_1|$  and  $\langle k_2|$  and using that  $\langle k_1|k_2\rangle = \delta_{1,2}$ , we obtain:

$$\alpha E_1 = \alpha \langle k_1|H_1|k_1\rangle + \beta \langle k_1|H_1|k_2\rangle \quad (12)$$

$$\beta E_1 = \alpha \langle k_2|H_1|k_1\rangle + \beta \langle k_2|H_1|k_2\rangle \quad (13)$$

In other words and in general, for any number of degenerate orthonormal eigenvectors  $|k_i\rangle$  with the same eigenvalue, the corrections  $E_1$  to the initial eigenvalue  $E_0$  are given by the eigenvalues of the matrix  $M$ , which is the matrix representation of  $H_1$  in the  $E_0$ -subspace, or, explicitly

$$M_{ij} = \langle k_i|H_1|k_j\rangle \quad (14)$$

The eigenvectors of  $M$  provide the linear combination of  $|k_i\rangle$  with a eigenvalue  $E_1^i$ . By construction  $M$  is hermitian  $M_{ij} = M_{ji}^*$  and the eigenvalues  $E_1^i$  are real.

What is left is to obtain  $M$ , which is done by

$$\begin{aligned} \langle k_i|H_1|k_j\rangle &= \langle k_i| \left( \sum_{n=0}^{N-1} |n\rangle\langle n| \right) H_1 \left( \sum_{n=0}^{N-1} |n'\rangle\langle n'| \right) |k_j\rangle \\ &= \sum_{n=0}^{N-1} \sum_{n'=0}^{N-1} \langle k_i|n\rangle\langle n|H_1|n'\rangle\langle n'|k_j\rangle \end{aligned} \quad (15)$$

In our case  $H_1|n\rangle = \cos(hn)|n\rangle$  and  $\langle n|H_1|n'\rangle = \cos(hn)\delta_{n,n'}$ . Therefore, we obtain:

$$\langle k_i|H_1|k_j\rangle = \frac{1}{N} \sum_{n=0}^{N-1} \exp(i\frac{2\pi k_i n}{N}) \cos(hn) \exp(-i\frac{2\pi k_j n}{N}) \quad (16)$$

If  $h = 2\pi m$ , with  $m$  integer, then  $\langle k_i|H_1|k_i\rangle = 1$ , but it is a case of no interest, as the system would have again unit lattice distance (or less). Otherwise, if  $h \neq 2\pi m$ :

$$\langle k_i|H_1|k_i\rangle = \frac{1}{N} \sum_{n=0}^{N-1} \cos(hn). \quad (17)$$

As it does not depend on  $k_i$ , the diagonal terms of  $M$  are equal and real, given by:

$$a = M(1,1) = M(2,2) = \Re \left( \frac{1}{N} \sum_{n=0}^{N-1} \exp(ihn) \right). \quad (18)$$

Let us call  $b = M(1,2) = M(2,1)^*$ , then, the eigenvalues of  $M$  are  $E_1 = \Delta\omega^2 = a \pm |b|$ . The value  $a$  represents a global shift of the dispersion curve, while  $b$  represents the separation in two values of  $\omega^2$ .

However, the term (18) is bounded by 1 at  $h = 0$ , which is of no interest. It is also zero for  $h = 2\pi/L$  with  $L = N/R$ ,  $L$  and  $R$  integers. For other values of  $h > 0$  it is very small except at the proximity of  $h = 0$ . Therefore, the global shift provided by the modulation is very small.

The non-diagonal elements of  $M$  are complex conjugates and given by:

$$\begin{aligned} b &= \langle k|H_1| - k \rangle = \frac{1}{N} \sum_{n=0}^{N-1} \exp(i2q_k n) \cos(hn) \\ &= \frac{1}{2N} \sum_{n=0}^{N-1} \exp(i[2q_k + h]n) + \frac{1}{2N} \sum_{n=0}^{N-1} \exp(i[2q_k - h]n). \end{aligned} \quad (19)$$

This expression is bounded by 1, taking its maximum absolute value 1 when both  $2q_k$  and  $h$  are integer multiples of  $2\pi$ . But that case is of no interest as it implies  $L = 1$  with no symmetry breaking, so  $h \leq \pi$ . However,  $b$  is close to 0.5 if at least one of the two sums in (19) is  $N$ , which happens for either  $2q_k + h = 2\pi m$  or  $2q_k - h = 2\pi m'$ , for  $m$  and  $m'$  integers. This condition is fulfilled for  $q_k \in [0, 2\pi]$  at four values, although they degenerate to a single value when  $h = \pi$  as  $-h/2 = h/2 - \pi$ .

Therefore if  $h < \pi$ :

$$b = M(1, 2) = \langle k|H_1| - k \rangle \simeq 0.5 \quad \text{for} \\ q = \frac{h}{2}, q = \frac{h}{2} + \pi, q = 2\pi - \frac{h}{2}, q = \pi - \frac{h}{2}. \quad (20)$$

Therefore, the effect of the modulations is a small shift in  $\omega^2(q)$  of order  $\delta a$  and the degeneracy raising of the bands for the four given specific wavenumbers is of order  $\delta/2$ .

As an example, if  $h = 2\pi/3$ , then  $a = 0$ , and the values of  $q$  for which the bands split are  $\pi/3, 2\pi/3, 4\pi/3, 5\pi/3$ . Figure 3 shows the numerically obtained dispersion function and the theoretical results on degeneracy raising. Note that the dispersion curves are represented within the Brillouin zone before modulation  $[0, 2\pi]$ . The Brillouin zone after modulation is  $[0, 2\pi/L] = [0, 2\pi/3]$ , with  $L = 3$  the new lattice distance after the breaking of the symmetry invariance. Phonon wavevectors  $q > 2\pi/3$  have to be translated to  $q - n2\pi/3$ , with  $n=1$  or  $2$ , to the new Brillouin zone. We think that this extended representation is clearer for the present context.

### III.B. Effect of only time modulation on the phonon bands

When  $h = 0$ , the effect of time modulation is to split the phonon band in several parallel bands separated by a frequency of  $\Omega$ . The number of bands diminishes with increased frequency and eventually the bands disappear or are not visible. Extra bands appear for frequency below  $\omega_0 = 1$  although they are very weak when approaching  $\Omega = \omega_0$ . Frequencies multiples of  $\omega_0$  lead to a divergence of the system. Frequencies inside the phonon band excites the modes with that frequency.

In the following we will use the notation and theory exposed in Appendix A, taking into account the changes brought about by the time dependence of the on-site potential.

### III.C. Breakup of the time-invariance: first approximation

Consider the unmodulated version of Eq. (7)

$$\ddot{u}_n = -\omega_0^2 u_n + \kappa(u_{n+1} + u_{n-1} - 2u_n). \quad (21)$$

It is invariant under translations in time  $t \rightarrow t + \Delta t$ , where  $\Delta t$  is the sampling interval, which could be arbitrary, in principle. Let us choose  $\Delta t = T_m/M$ , with  $M$  an integer, that is  $\Omega = 2\pi/T_m = M2\pi/\Delta t$ . The addition of the term  $-\delta \cos(\Omega t)u_n$  to the rhs of (21) breaks this invariance. The modulated system is invariant only under larger translation of time  $T_m = M\Delta t$ , multiples of  $\Delta t$ . There is a breaking of the symmetry to a smaller symmetry.

The new solution is given by Bloch theorem<sup>15,16</sup>, as  $\exp(-i\omega t)$ , multiplied by a periodic function with the pe-

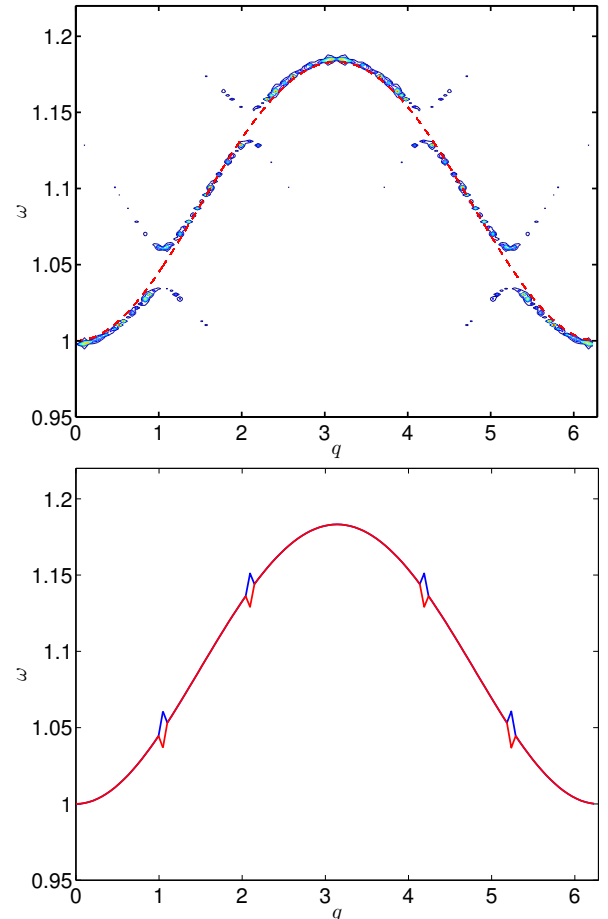


FIG. 3. (Top:) Numerical dispersion bands for  $h = 2\pi/3$ ; (Bottom:) Theoretical degeneracy raising of the dispersion bands due to space modulation. Note that the Brillouin zone is  $[0, 2\pi/3]$ . See the text for explanation.

riod of the operator, that is

$$u = \exp(i[qn - \omega t]) \sum_{m=-M/2}^{M/2} A_m \exp(-im\Omega t),$$

with the coefficients  $A_m$  depending on  $q$ .

Then, the substitution of  $u$  into the dynamical system leads to (substituting  $\cos(\Omega t) = (\exp(i\Omega t) + \exp(-i\Omega t))/2$ ):

$$(\omega + m\Omega)^2 A_m = [\omega_0^2 + 2\kappa(1 - \cos(q))] A_m \\ + \frac{\delta}{2}(A_{m+1} + A_{m-1}), \quad (22)$$

or

$$(\omega + m\Omega)^2 A_m = \bar{\omega}_q^2 A_m + \frac{\delta}{2}(A_{m+1} + A_{m-1}), \quad (23)$$

where  $\bar{\omega}_q$  is the unperturbed frequency for the wavenumber  $q$ . This is a complicated equation, but if  $\delta$  is small

with respect to  $\Omega$ , we can suppress that term in the first approximation, that is.

$$(\omega + m\Omega)^2 A_m = \bar{\omega}_q^2 A_m. \quad (24)$$

This equation has a solution corresponding to make all  $A_k = 0$ , except  $A_m$ , for each  $m$ , indicating that each solution is characterized by a harmonic of higher order of the modulating wave.

Then, we obtain:

$$\omega_{q,m} = -m\Omega + \sqrt{\bar{\omega}_q^2} = -m\Omega + \sqrt{\omega_0^2 + 2\kappa(1 - \cos(q))}. \quad (25)$$

Therefore, the main effect of the symmetry breaking is the apparition of bands separated by the frequency  $\Omega$  almost parallel to the unperturbed dispersion band (UDB). However, the intensity of those bands tend to be smaller the further apart from the UDB. It is necessary to plot contours of small intensity in order to observe them.

Solving (24), it is also possible to obtain  $\omega = m\Omega - \bar{\omega}_q^2$ , but this equation lead to a change of sign of the frequencies, corresponding to waves traveling in opposite direction, which are already obtained for negative wavenumbers  $q$ .

Two examples can be seen in Fig. 4

### III.D. Dispersion bands for space-time modulation

Considering the system (7):

$$\ddot{u}_n = -\omega_0^2 u_n - \delta \cos(hn - \Omega t) u_n + \kappa(u_{n+1} + u_{n-1} - 2u_n). \quad (26)$$

The system is now  $2\pi$  periodic in the variable  $hn - \Omega t$ , and the solutions can be written as the product of a plane wave multiplied by a function with the periodicity of the system. That is:

$$u = \exp(i[qn - \omega t]) \sum_{m=-M/2}^{M/2} A_m \exp(im[hn - \Omega t]).$$

Then, the substitution of  $u$  in the Hamiltonian leads to (substituting  $\cos(hn - \Omega t) = (\exp(i[hn - \Omega t]) + \exp(-i[hn - \Omega t]))/2$ ):

$$(\omega + m\Omega)^2 A_m = [\omega_0^2 + 2\kappa(1 - \cos(q + mh))] A_m + \frac{\delta}{2}(A_{m+1} + A_{m-1}). \quad (27)$$

Assuming that  $\delta$  is small with respect to  $\Omega$ , we can obtain the independent solutions where all the  $A_k = 0$ , except one  $A_m$  each time, so it correspond to a single harmonic with  $\omega$ :

$$\omega = -m\Omega + \sqrt{\omega_0^2 + 2\kappa(1 - \cos(q + mh))} \quad (28)$$

An example can be seen in Fig. 5.

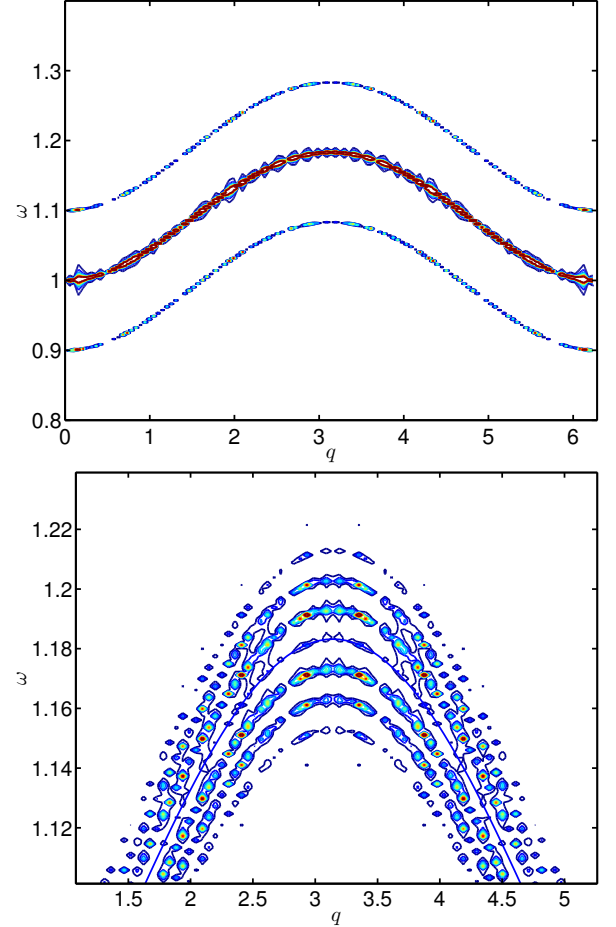


FIG. 4. (Top) Contour plot of the 2DFFT for  $\delta = 0.05$ ,  $\Omega = 0.1$ ,  $\kappa = 0.1$  (Bottom) Identical parameters except  $\Omega = 0.01$

## IV. BREATHERS WITH SPACE-TIME MODULATION

In this section we study the conditions for breather existence in a modulate system, first reviewing the theory of exact breathers in<sup>17</sup> and adapting it to space-time modulation and to just time modulation.

### IV.A. Theory of exact traveling breathers

In this section we follow closely the theory developed in Ref.<sup>17</sup>. Let us suppose that we have a space time modulated system with phase  $\phi = hn - \Omega t$  and velocity  $V_m = h/\Omega$ . An exact breather will be a solution of the form

$$u(n, t) = f(n - V_b t, \omega_F t), \quad (29)$$

where  $\omega_F = 2\pi/T_F$  is the fundamental frequency,  $T_F$  is the fundamental period, defined as the minimal time for which  $u$  reproduces itself displaced a distance  $s = V_b T_F$  called the step. The function  $f$  is a localized function

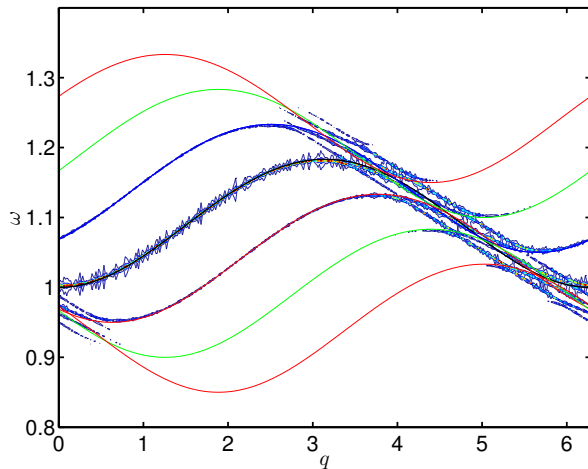


FIG. 5. Contour plot of the FFT2 for  $\delta = 0.05$ ,  $\Omega = 0.05$ ,  $\kappa = 0.1$  and the theoretical dispersion relation lines: Note that there is an area to the right where the harmonics are very close and become mixed.

of its first argument and a  $2\pi$  periodic function of the second. The frequency  $\omega_i$  is the moving frame or internal frequency for short.

The condition for  $u(n, t)$  to be exact is that  $u(n + s, t + T_F) = u(n, t)$ , which implies that  $s = V_b T_F$  and  $\omega_i = m\omega_F$ . Harmonic functions with the same symmetry (same step and fundamental frequency) are called resonant harmonics and form a basis for the breather. They can be written as

$$\exp(i(q[n - V_b t]) \exp(-im\omega_F t) = \exp(i[qn - \omega_L t]) \\ \text{with } \omega_L = qV_b + m\omega_F. \quad (30)$$

where  $\omega_L$  and  $m\omega_f$  are the laboratory and moving frame frequencies, respectively, of the resonant harmonic.

The resonant harmonics form straight lines within the  $(q, \omega)$  space, called *resonant lines*. Their slope is  $V_b$  and their intercept at the axis  $q = 0$  is  $m\omega$ , i.e, the moving frame frequency. Therefore, all the harmonics in a resonant line have the same frequency  $m\omega_F$ , with the integer  $m$  indexing the lines.

The breather frequencies are inside one of those lines called the *breather line* with  $m = m_b$ . The intercept of the breather line with the axis  $q = 0$  is the moving frame frequency of the breather  $\omega_b = m_b\omega_F$ . All the harmonic waves in the same line have the same frequency in the moving frame and propagates with the same velocity  $V_b$ , which explains the persistence of the breather.

For a soft potential as in our case, the breather line will be below the phonon band, and close to its minimum at  $q = 0$ . If the breather line intersects the phonon band, the intersection phonon will be excited leading to a wing, an extended quasi-linear harmonic wave attached to the breather, with amplitude depending on the specific system and the frequency, and sometimes being zero.

#### IV.B. Application to space-time harmonically modulated systems

For a space-time harmonically modulated system with a term  $\cos(hn - \Omega t)$ , it is also necessary that the value of the modulating phase  $\Phi = hn - \Omega t$  is also identical modulo  $2\pi$  after the translation  $s$  and time change  $T_F$ , because if not, the forces will be different and the evolution of  $u$  would be different.

Therefore:

$$h(n + s) - \Omega(t + T_F) = hn - \Omega t + 2\pi m_m \rightarrow \\ \Omega = \frac{hs + 2\pi r}{T_F} \rightarrow \Omega = hV_b + m_m\omega_F. \quad (31)$$

This means that the modulating wave is a resonant harmonic with index  $m_m$  and moving frame frequency  $m_m\omega_F$  and therefore the breather and modulating waves have commensurate moving frame frequencies.

**Lemma 1** *A necessary condition for an exact breather within a space-time modulated system with harmonic modulation is that the modulating harmonic is within a resonant line with the breather, or, in other words, that their moving frame frequencies are both integer multiples of the fundamental frequency  $\omega_F$ . Therefore  $\omega_b$  and  $\Omega$  are commensurate.*

The immediate consequence for only time modulation is:

**Lemma 2** *For a harmonically, time-modulated system, a necessary condition for breather existence is that the breather frequency  $\omega_b$  and the modulating frequency  $\Omega$  are commensurate:  $\omega_b/\Omega = m_b/m_m$ .*

#### IV.C. Breather obtention in the time-modulated system

The most direct way is working on the real space with the Newton and shooting method. Trying some different localized initial conditions and observing an approximate periodical behavior with period close to  $T_b$ , the intended one, the initial conditions are used as a seed for the Newton method where initial conditions corresponding to the exact  $T_b$  periodic behavior. Exact means with a precision of  $10^{-15}$ , that is, very close, to the computer machine precision. The Newton method, a numerical application of the implicit function theorem, can be used as the system has no time invariance due to the time-periodic term in the potential, and a solution is unique in its neighborhood. The precision can be refined more by working in the space of the frequencies, if we consider time-reversible solutions, they can be written as  $u_n(t) = \sum_{k=-k_m}^{k_m} z_{k,n} \exp(k\omega_b t)$ . Due to  $u_n(t)$  being real and time-symmetric,  $z_{k,n}^* = z_{-k,n}$  and  $z_{k,n} = z_{-k,n}$ , and real. The  $u_n(t) = z_{0,n} + \sum_{k=1}^{k_m} 2z_{k,n} \cos(k\omega_b t)$ , being  $2z_k, n$  the inverse cosine fast Fourier cosine transform (idfc). Then, the Newton method can be coded in the space of the  $k_m + 1$  FFT components, finding the fftc

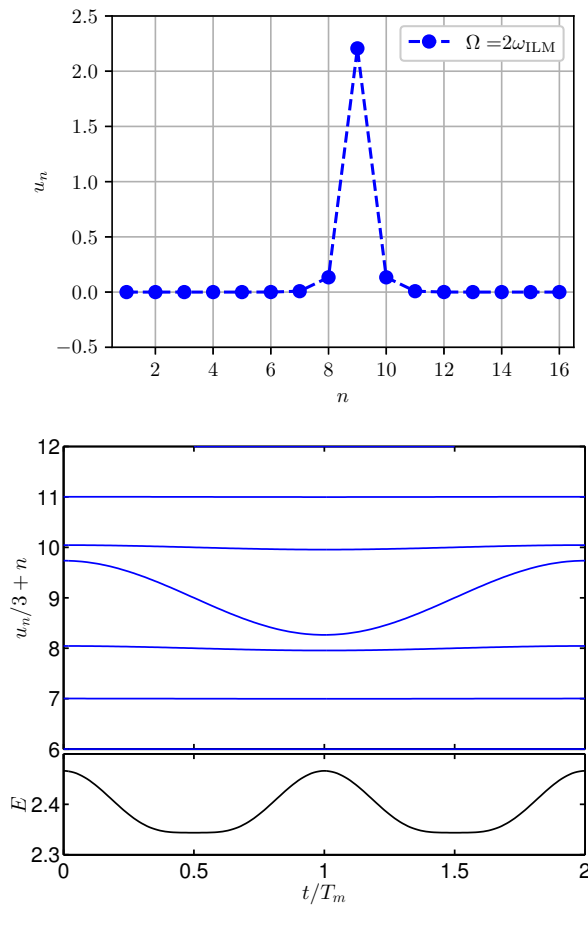


FIG. 6. (Top) For  $\Omega = 2\omega_b$ , profile of the stable breather. (Bottom) Coordinates and energy evolution in a breather period  $T_b$ .

components  $z_{n,k}$ . The value of  $m = 15$  provides excellent results.

The breather initial coordinates for the case  $\Omega = 2\omega_b$  are represented in Fig. 6-top, the initial velocities being zero.

#### IV.D. Stability of breathers in the time-modulated system

Let us suppose that the breather solution for a time crystals with  $T_b = n_T T_m$ , with  $n_T$  an integer larger than 1, the  $T_m$ -periodic system is also  $T_b$  periodic, and to analyze the stability we can construct the Floquet matrix integrating a small perturbation of the initial coordinates and momentum and observing the perturbation after  $T = T_b$ . For each changed coordinate we obtain a column of the Floquet matrix  $F$ . Its eigenvalues lie at the unit circle if the system is stable. For autonomous systems symplectic systems<sup>18</sup> there are always two eigenvalues of  $F$  at  $+1$ , corresponding to  $u_t = \dot{u}$ , the phase mode, as it represents that if  $u(t)$  is a  $T_b$  periodic solution,  $u(t +$

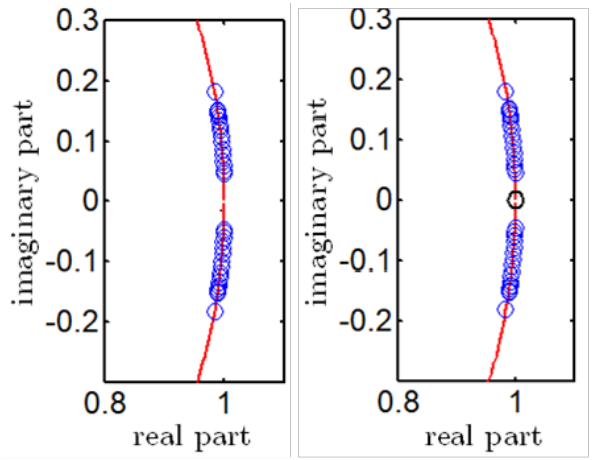


FIG. 7. For  $\Omega = 2\omega_b$  Floquet multipliers (left) for the non-autonomous system and (right) for the extended autonomous system. See text.

$dt$ ) is also a solution, and the growth mode, indicating that around a solution there is another one with slightly different amplitude.

Those two eigenvalues do not generally appear for the non-autonomous system as can be seen in Fig. 7-left for  $\Omega = 2\omega_b$ . The explanation is that if we write the dynamical equations (9) in a condensed form as:

$$\ddot{u}_n - L_n u_n + (1 + \delta_2 \cos(\Omega t)) \frac{\partial V(u_n)}{\partial u_n} = 0, \quad (32)$$

where  $L_n u = -\omega_1^2 u_n + \kappa(u_{n+1} + u_{n-1} - 2u_n)$ , with  $\omega_1^2 = \omega_0^2 - \delta_1 = \omega_0^2 - 1/d_0^3$ , being the linear, unmodulated part of the dynamical system, with  $V(0) = 0$ ; and  $V(u_n) = 1/d_0 - 1/\sqrt{d_0^2 + u_n^2}$ , the local non-modulated on-site potential.

If  $u_b(t)$  is a  $T_b$ -periodic solution of (32), and  $u(t) = u_b(t) + \xi(t)$  a perturbed solution with  $\xi(t)$  small, the evolution of  $\xi$  is given by the Newton operator with zero eigenvalue, that is:

$$\begin{aligned} N_n \xi &= \ddot{\xi}_n - L_n \xi \\ &+ (1 + \delta_2 \cos(\Omega t)) \frac{\partial^2 V(u_{b,n}(t))}{\partial u_n^2} \xi_n = 0. \end{aligned} \quad (33)$$

For autonomous systems  $\dot{u}_b$  is a solution of (33), but not for non-autonomous ones, as the derivative of (32) is given by:

$$\begin{aligned} \ddot{u}_{b,n} - L_n \dot{u}_{b,n} \\ + (1 + \delta_2 \cos(\Omega t)) \frac{\partial^2 V(u_{b,n}(t))}{\partial u_n^2} \dot{u}_{b,n} \\ - \Omega \delta_2 \sin(\Omega t) \frac{\partial V(u_{b,n}(t))}{\partial u_n} = 0, \end{aligned} \quad (34)$$

where the last term does not appear in (33).

However, it can be recovered within an autonomous extended system that includes the autonomous one as it is shown below. For the different factors  $n_T$ , in  $\Omega = n_T \omega_b$ , we obtain different results that we will present later.

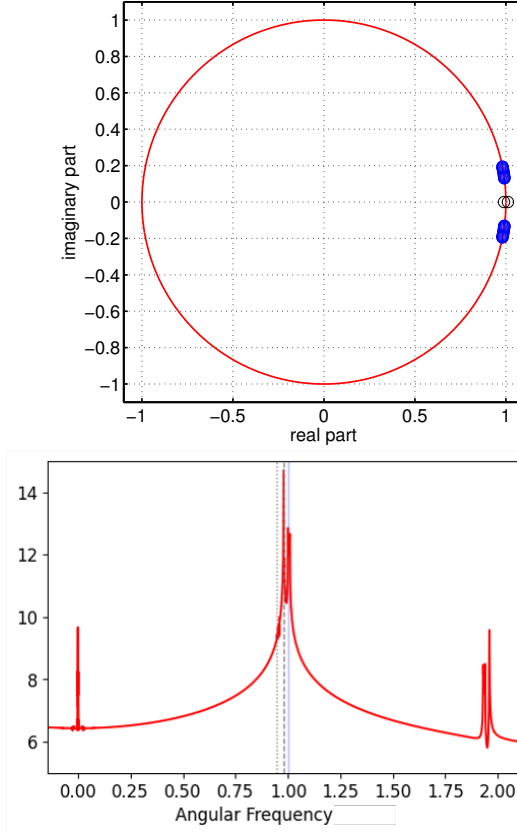


FIG. 8. (Top) Floquet eigenvalues for a breather with  $\Omega = 3\omega_b$  and  $\omega_b = 0.98$  (Bottom) Fourier spectra of the same breather embedded in a noisy system with  $N = 160$  cantilevers.

#### IV.E. Extended autonomous symplectic system

The Hamiltonian structure of the dynamical equations, i.e.,  $\dot{u}_n = \partial H / \partial p_n$ ,  $\dot{p}_n = -\partial H / \partial u_n$  is kept for the conjugate pairs of variables  $u_n$ ,  $p_n$ , although the system is no longer autonomous. By defining  $s = t$  or to be precise as (33) is  $T_b$ -periodic, as  $s = \text{rem}(t, T_b)$ , the remainder of  $t/T_b$ , i.e.,  $\text{rem}(nT_b + t, T_b) = t$  and  $\text{rem}(-nT_b - t, T_b) = -t$ , both for  $n > 0$  and  $t > 0$ , so as  $s$  is  $T_b$  periodic. Then  $\dot{s} = 1$  as usual, and the system with the extra variable has become autonomous, but not symplectic as  $s$  has no conjugate variable yet. The extra variable  $h$  to make the system symplectic is obtained by defining a new Hamiltonian  $K = H + h$ , with  $h$  the conjugate momentum of  $s$  as  $\dot{s} = \partial K / \partial h = 1$  as previously obtained.

Then,  $\dot{h} = -\partial K / \partial s = -\partial H / \partial s = -\partial H / \partial t = -dH/dt$ , or  $h = E_0 - H$ , with  $E_0$  the initial energy at  $t = 0$ <sup>19</sup>. The extended system is now symplectic and  $[\dot{u}_b, \dot{s}]$  is now solution of (34) and being  $T_b$  periodic, the Floquet multiplier +1 corresponding to the *phase mode* reappears. There is an extra +1 multiplier, because, symplectiness, implies that the multipliers are in pairs  $\lambda, 1/\lambda$ , the extra mode corresponding to a solution with slightly different energy or *growth mode*.

The extended system reveals a hidden symplectic structure of the autonomous system with the implication that stability corresponds to all the Floquet multipliers being in the unit circle, but without the double multiplier of +1, which is recovered with the extended system. Figure 7-right shows these multipliers for  $\Omega = 2\omega_b$ .

Note these conclusions are valid both the cases  $\Omega > \omega_b$  and  $\Omega \leq \omega_b$  studied in the next two sections taking due care of the time of integration. They are also valid for space-time modulated systems with trivial changes that we will detail elsewhere.

#### V. TIME CRYSTALS: BREATHERS WITH TIME MODULATION AND $\Omega = n_T \omega_b$

We consider the nonlinear dynamical system (9) with two main cases,  $\omega_b = \Omega/n_T$  ( $T_b = n_T T_m$ ), and  $\omega_b = n_T \Omega$  ( $T_b = T_m/n_T$ ),  $n_T$  an integer. The first one correspond to time crystals<sup>20,21</sup>, while the latter has no specific name. Although, according to the deduction in Sec. IV, fractional frequencies are also possible, we will not consider them in this article. A condition for proper time crystals is the no production of entropy, which happens here as the energy is repeated after  $T_b$  with no energy dissipation as shown in Fig. 7.

In this section we consider time crystals and leave the condition of  $\Omega < \omega_b$  for the next section.

The dynamical equations (9) are invariant under the transformation  $t \rightarrow t + T_m$ , therefore, if a phonon  $(q, \omega)$ , i.e.,  $u = \exp(i[qn - \omega t])$  is a solution of the linearized equation, then also  $\exp(im\Omega t)u$  is also a solution, or, in other words, there is another phonon band with frequencies  $\omega' = \omega + m\Omega$ , with  $m$  a positive or negative integer. But there are also two phonon bands, with positive and negative frequencies, then, if there is a phonon  $(q, \omega)$ , also there exists the phonon  $(q, \Omega - \omega)$ . As the unmodulated phonon band is  $\in [\omega_0 = 1, \omega_{\max} = 1.01$ , for  $\Omega \simeq 2$ , a new phonon band appears  $\in [\Omega - \omega_{\max} \simeq 0.98, \Omega - \omega_0 \simeq 1]$ . The phonon bands in the modulated system change position, and  $\Omega = 2\omega_b = 1.96$ , but those bands are very close with the possibility of interfering, depending on the exact value of  $\omega_b$  and actual modulated phonons. This problem does not exist for  $\Omega \geq 3$  as the band  $\Omega - \omega_{\text{phon}}$  is much separated.

For  $\Omega = 2\omega_b$ , and changing slightly  $\omega_b$ , there is an interval where the two phonon bands coincide and then the system becomes stimulated by  $\Omega$  and the variables diverge. A dissipation term can be added, but as this a

very special case, we prefer not to modify the system and simply avoid those combination of frequencies.

### V.A. Period doubling $\Omega = 2\omega_b$

In the figures we can see the profile of breather and neighbors, also the evolution of the energy, which is  $T_m$ -periodic and therefore also  $T_b$ -periodic. There is no net gain or loss of energy every period, which indicates that the solution is a true time-crystal. The Floquet eigenvalues are also pictured. The eigenvalues corresponding to the phonons form a pair of complex conjugate bands width frequencies  $\omega_i = \omega_b + \theta_i/T_b$ , as they have the same Krein signature<sup>18</sup> they form a structurally stable subset. There is also a close but separate eigenvalue with a localized eigenvector, and thus corresponding to the breather solution. It has the opposite Krein signature of the phonons, meaning it can collide with the phonon with closest frequency leaving the unit circle, which indicates that the breather is unstable and another solution exists, most likely and extended one, corresponding to the merger of the breather with the upper phonon mode.

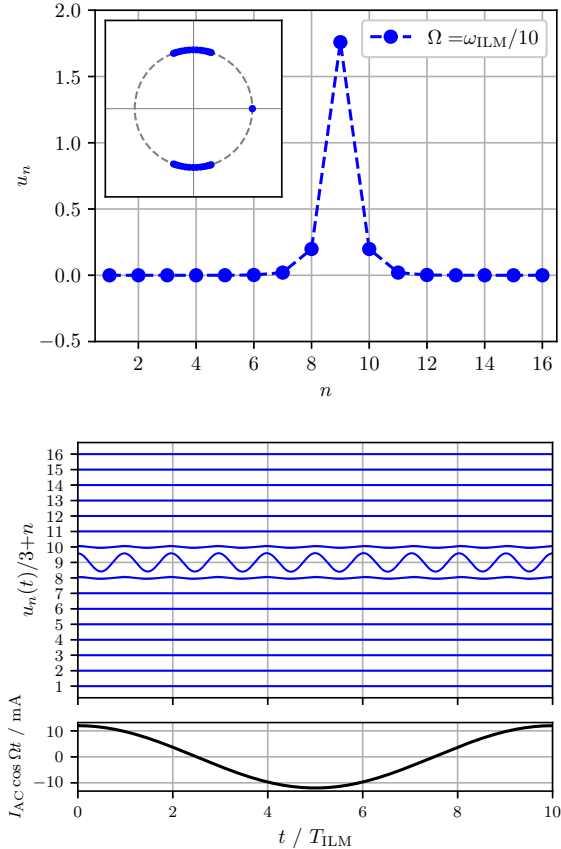


FIG. 9. (Top) Profile and Floquet eigenvalues for a breather with  $\Omega = \omega_b/10$  and  $\omega_b = 0.98$  (Bottom) Evolution of the coordinates and the AC current.

### V.B. Cases $\omega_b = 3\Omega$ to $\omega_b = 10\Omega$

For  $\omega_b = 3\Omega$  the breather is slightly unstable with two real multipliers very close to +1. In spite of that simulations can be done to simulate the breather evolution with relatively long time. The Floquet multipliers are represented in Fig. 8 and the Fourier spectrum in a system with noise and  $N = 160$  oscillators are shown.

For  $\omega_b = n_T\Omega$ , width  $n_T = 1 \dots 10$ , we have constructed breathers, for  $n_T = 3, 4, 8$  breathers are unstable, while the rest are stable, therefore there is no apparent pattern. For example, for  $n_T = 3$ , there are two two real eigenvalues slightly separated from +1, but, in spite of that, the breather has a long life.

### VI. BREATHERS WITH $\Omega = \omega_b/n_T$

A peculiarity of this case is that the stability of the breather and the Floquet matrix have to be calculated for a time equal to the modulation period  $T_m = n_T T_b$  as the coordinates, and velocities have to repeat but also the forces which depend on time an only repeat after  $T_m$ . Therefore, the phonon band appear with Floquet exponents multiplied by  $n_T$  and spread out they are given  $\theta_q = \omega_q T_m = n_T \omega_q T_b$  for a phonon of frequency  $\omega_q$ .

In this section we separate the study of the Sievers-Takeno mode<sup>22</sup> or single breather, from the Page mode<sup>3</sup>, or double breather. Values  $n_T = 1, 2, \dots, 32$  are considered and a breather obtained. For  $n_T = 32, \dots, 40$  phonobreathers appear as explained in Sec. VI VI.B.

#### VI.A. Sievers-Takeno mode: single ILM with $\omega_b = n_T\Omega$

A stationary, single ILM or breather is a localized periodic vibration with a given frequency  $\omega_b$  and with a single site, that we call the central one, having a large amplitude with respect to the phonons, and the amplitude of the neighbors diminishing rapidly with their distance to the center. They are often constructed from the anti-continuous limit with a single excited oscillator and the other at rest<sup>23-25</sup>

In our system, the unmodulated system dispersion relation is given by  $\omega^2 = \omega_0^2 + 2\kappa(1 - \cos(q))$ , with a minimum frequency  $\omega_0 = 1$ . As the nonlinear part of the on-site potential is soft, because the dominant term is  $o(3)$ , stationary breathers or ILMs will have a frequency  $\omega_b$  below the minimum frequency  $\omega_0$ . As demonstrated in Sect. IV, for a time-modulated system, the modulating frequency  $\Omega$ , is commensurate with  $\omega_b$ , and in this subsection, we consider the case  $\Omega = \omega_b/n_T$ . By using the shooting method, we tried and obtained exact ILMs for many values of  $n_T$ , as 1, 2, … 40. We present here only some results with  $\omega_b = 0.98$ , that is, very close to the minimum frequency  $\omega_0 = 1$  for the unmodulated system.

We construct the ILM in a small lattice with  $N = 16$  cantilevers, and check its stability by constructing the

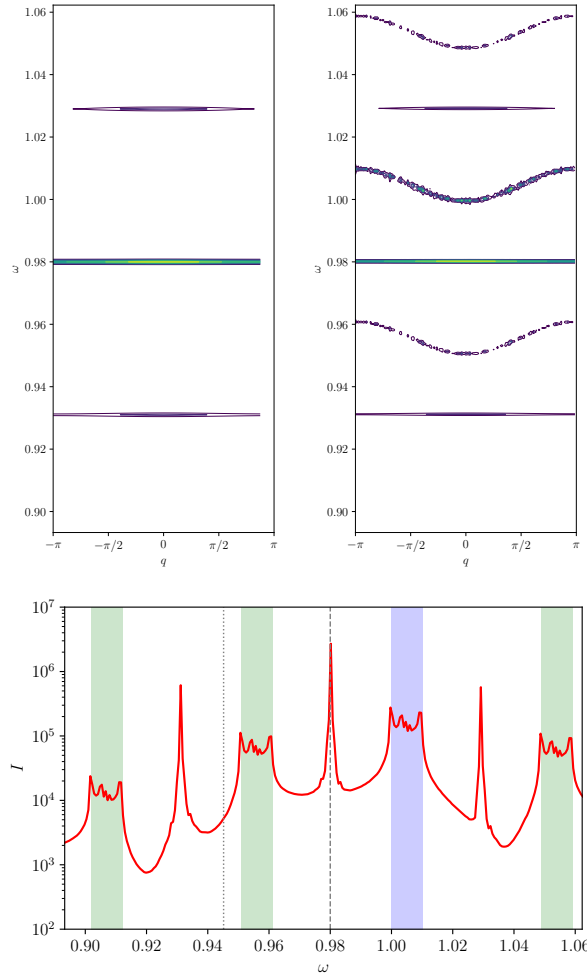


FIG. 10. Case  $\Omega = \omega_b/20$  and  $\omega_b = 0.98$  (Top) Frequency-momenta representation with scaled frequency. To the left for  $N = 16$  sites, and to the right for  $N = 160$  and noise added. See text. (Bottom) Spectra of the Fourier intensities in arbitrary units with respect to the scaled frequency. See text.

monodromy matrix and obtaining the Floquet multipliers and exponents<sup>18</sup>. Then we embed the initial positions and within a larger lattice with  $N = 160$  particles with some small random noise velocities, let it evolve and perform the 2D FFT to check the results. An example  $\Omega = \omega_b/10$  with  $\omega_b = 0.98$  can be seen in Fig. 9. The top panel shows the profile at  $t = 0$  and the Floquet eigenvalues, showing its stability. The bottom panel illustrates the evolution of the variables for a period of the AC current.

We choose the case  $\Omega = \omega_b/20$  with  $\omega_b = 0.98$ , to illustrate the frequency-momenta representation as it is more easily seen. The top panel of Fig. 10-top shows the theoretical spectra  $\omega = \pm m\Omega + \sqrt{\omega_0^2 + 2\kappa(1 - \cos(q))}$ . The horizontal dotted line is the scaled physical frequency  $\omega_0/\omega_{0,\text{phys}}$  of an isolated oscillator without modulation

for reference (See Sect. II). To the right it is shown the numerical spectra obtained for the larger lattice with some noise added that makes the dispersion relation to appear. The figure is obtained by adding up the intensities for all the particles at the same time.

We can see that also that frequencies  $\omega_b \pm \Omega$  appear displaced  $\omega_0 - \omega_b = 1 - 0.98 = 0.02$  above and below the bottom of the secondary dispersion curves. Horizontal lines for the ILM are due to the extreme localization in  $u_n$  and consequent dispersion in  $q$ .

Figure 10-bottom shows the spectra intensity with respect to the frequency, where the phonon bands and the extra ILM bands can also be observed. The upper and lower secondary phonon and ILM bands are symmetric, there are more secondary bands for  $m > 1$  with diminishing intensities.

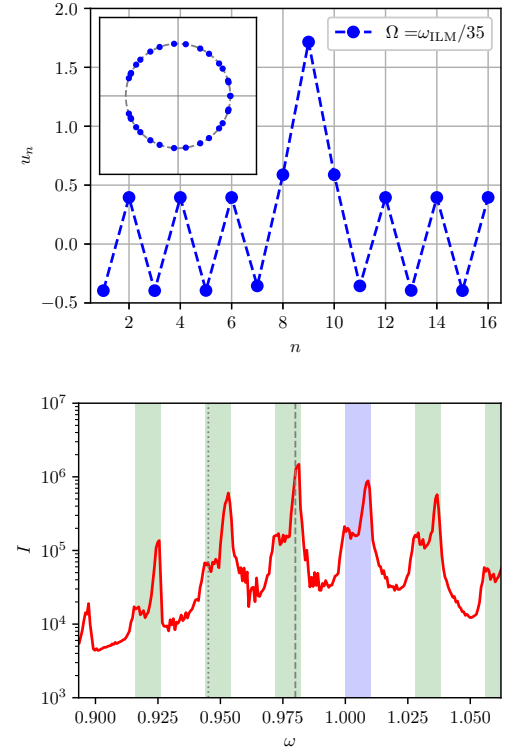


FIG. 11. (Top) For  $\Omega < \omega_b/33$ , a phonobreather appears as a background to the ILM. (Bottom) Fourier spectra. See text.

### VI.B. Single ILM with phonobreather background for $\omega_b = n_T \Omega$

Although the obtention of ILM for increasing  $n_T$  is possible, as  $\Omega$  becomes smaller, the upper secondary ILM band  $\omega_b + \Omega$  collides with the upper frequency of the phonon band  $\omega_{\text{max}} = \sqrt{\omega_0 + 2\kappa(1 - \cos(\pi))} = \sqrt{\omega_0 + 4\kappa} = \omega_b + \Omega$ , or  $\Omega = \omega_{\text{max}} - \omega_b$  and  $\omega_b/\Omega \simeq 32.3$ . Then for  $n_T > 30$  the upper phonons are excited and a

phonobreather<sup>26</sup> with  $q = \pi$  profile appears as the background of the ILM, with smaller but comparable amplitude. A phonobreather is a periodic solution on a nonlinear system with homogeneous amplitude. It is not a phonon as it is not a solution of the linearized system and has a significant amplitude. It can also be described as a nonlinear extended wave.

The profile of the breather with phonobreather background can be seen in Fig. 11-(Top) and at the bottom of the same figure, the Fourier spectra, where the colliding of the top of the phonon bands can be seen merging with the ILM bands of upper order, while in Fig. 10-bottom they are well separated.

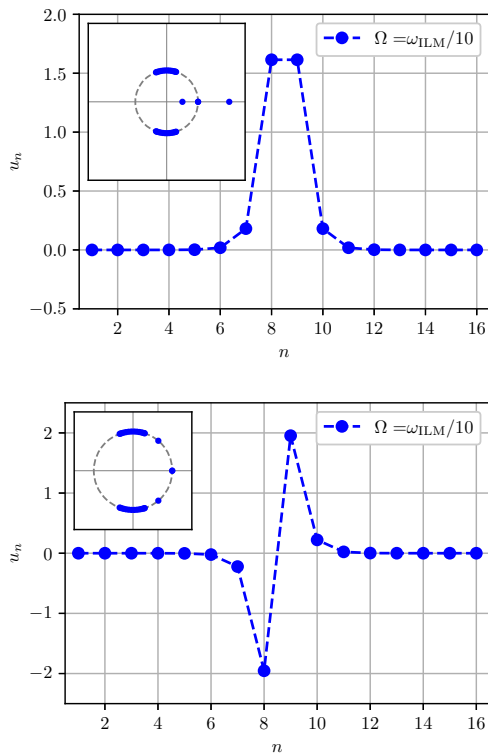


FIG. 12. (Top) For  $\Omega < \omega_b/10$ , profile of the unstable in-phase Page mode. (Bottom) The stable anti-phase Page mode with the same parameters and modulating frequency.

### VI.C. Page modes with $\omega_b = n_T \Omega$

A Page mode<sup>3,4</sup> is a double breather or ILM with two sites vibrating with the same amplitude, it can be bond-symmetric if both sites oscillate in-phase (iP), or bond-antisymmetric if they oscillate in anti-phase (aP). The iP mode is unstable and the aP is stable for an unmodulated Klein Gordon system with soft potential<sup>26</sup>. Both two modes appear also in the modulated system with the same stability properties. Both mode profiles and Floquet multipliers are represented in Fig. 12 for  $\omega_b = 10\Omega$ .

The 2DFFT of the in-phase mode shows the appearance of another breather band closer to the bottom of the phonon band, which correspond to a the unstable mode. Similar phenomena to the single ILM occur, i.e., formation of replicas of the phonon band and ILM band displaced  $\pm\Omega$  in the frequency space and the excitation of a phonobreather background when the secondary ILM band interacts with another replica of the phonon band just below.

## VII. CONCLUSIONS

We have modified a previous system corresponding to a physical model of cantilever arrays with on-site potential provide by electromagnets so as the on-site potential can be modulated both in time and space with DC and AC currents.

We have deduced their equations both in the linear and nonlinear range. We have obtained theoretically and observed numerically the change in the dispersion bands for space and time modulation separately and together. We have adapted the theory of exact breathers to time-modulated systems deducing that the modulation and breather frequencies in the moving frame should be commensurate as a necessary condition for breather existence.

We have analyzed the peculiarities of the stability analysis for time-modulated systems with the construction of and extended symplectic system. Time-crystal breathers, that is, breathers with a period multiple of the modulating system are observed and their properties analyzed.

For the modulating frequency smaller than the breather's one, we have found single breathers and double breathers, both symmetric and anti-symmetric. When the modulating frequency becomes small a phonobreather background appear.

The study reveals that this relatively simple system provides a great variety of breather solutions which may also appears in other space-time modulated materials also known as dynamic metamaterials<sup>27</sup>.

## ACKNOWLEDGEMENTS

JFRA acknowledges the Laboratory of Microdynamics at the University of Osaka for hospitality.

## FUNDING

JFRA and VJSM thanks grant PID2022-138321NB-C22 funded by MICIU/AEI/ 10.13039/501100011033 and ERDF/EU.

MK acknowledges support from JSPS Kakenhi (C) No. 24K07393 and 21K03935.

YD acknowledges support from JSPS Kakenhi (C) No. 24K14978.

## Appendix A: Notation

To present formally the theory, we will use the ket and bra notation. The nice thing of that notation is that the properties of operations with vectors, change of basis, and operators appear as the simple juxtaposition of kets and bras. We present here this notation, more details can be read in Ref.<sup>13</sup> and in Ref.<sup>26</sup> applied to breather theory.

For our purposes, let us consider initially a ket  $|\phi\rangle$  as a vector which can be expressed in different bases. There are two bases of interest in the domain of  $H_0$ , the first one is given by  $|n\rangle$ 's, with  $n = 0 : N - 1$ , acting on any eigenfunction  $|u\rangle$  of  $H_0$  as  $\langle n|u\rangle = u_n$ . In that same basis is the column matrix  $|n\rangle = [0, 0, \dots, 0, 1, 0, \dots, 0]'$ , with the only 1 in position  $n$  and the rest zeros. A vector of positions are  $|u\rangle = [u_1, u_2, \dots, u_n]'$  can be seen as  $|u\rangle = \sum_{n=0}^{N-1} u_n |n\rangle$ .

The bra  $\langle\phi|$  is the Hermitian conjugate, so  $\langle\phi|$  is a row matrix with elements the complex conjugates of the elements of  $|\phi\rangle$ . In this way, a bracket  $\langle\phi_1|\phi_2\rangle$  is the scalar product  $\sum_{n=0}^{N-1} \phi_{1,n}^* \phi_{2,n}$ . Trivially  $\langle n|n' \rangle = \delta_{n,n'}$ . So the basis  $\{|n\rangle\}$  is orthonormal.  $\langle n|\phi\rangle = \phi_n$  as the scalar product by a unit basis vector and therefore the component of  $|\phi\rangle$  in the direction of the unitary vector, or the component in that basis.

A dyad  $|\phi_1\rangle\langle\phi_2|$  is a linear operator acting on kets as  $|\phi_1\rangle\langle\phi_2||\phi_3\rangle = \langle\phi_2|\phi_3\rangle|\phi_1\rangle$

Any linear operator  $H$  can be expressed in a given basis as a sum of dyads as  $H = \sum_{n=0}^{N-1} \sum_{n'=0}^{N-1} H_{n,n'} |n\rangle\langle n'|$ , with  $H_{n,n'} = \langle n|H|n'\rangle$  being the elements of the matrix representation of  $H$  in the basis  $\{|n\rangle\}$ .

The second basis is the momenta basis, and it is given in the  $\{|n\rangle\}$  basis as:

$$|q_k\rangle = |k\rangle = \frac{1}{\sqrt{N}} \sum_{n=0}^{N-1} \exp(-i\frac{2\pi kn}{N}) |n\rangle, \quad \text{then}$$

$$|n\rangle = \frac{1}{\sqrt{N}} \sum_{k=0}^{N-1} \exp(i\frac{2\pi kn}{N}) |k\rangle. \quad (\text{A1})$$

The second expression is the representation of  $|n\rangle$  in the  $|k\rangle$ -basis.

The following relations are useful and easy to obtain:

$$\langle n|n' \rangle = \delta_{n,n'} \quad ; \quad \langle k|k' \rangle = \delta_{k,k'} \quad ; \quad (\text{A2})$$

$$\langle k|n\rangle = \frac{1}{\sqrt{N}} \exp(i\frac{2\pi kn}{N}) \quad ; \quad \langle n|k\rangle = \frac{1}{\sqrt{N}} \exp(-i\frac{2\pi nk}{N}) \quad (\text{A3})$$

The identity operator is given by  $I = \sum_{n=0}^{N-1} |n\rangle\langle n| =$

$\sum_{k=0}^{N-1} |k\rangle\langle k|$ , then

$$|u\rangle = \sum_{n=0}^{N-1} |n\rangle\langle n|u\rangle = \sum_{n=0}^{N-1} u_n |n\rangle, \quad \text{and}$$

$$|u\rangle = \sum_{k=0}^{N-1} |k\rangle\langle k|u\rangle = \sum_{k=0}^{N-1} F_k(u) |k\rangle, \quad (\text{A4})$$

where  $\langle n|u\rangle = u_n$ , is the  $n$ -component of  $|u\rangle$  in the  $\{|n\rangle\}$  basis, and  $\langle k|u\rangle = F_k(u)$  is the  $k$ -component of  $|u\rangle$  in the  $|q_k\rangle$  basis.

Using the appropriate form of the identity operator we can obtain the relationship between  $u_n$  and  $F_k(u)$ , that is the inverse and direct discrete Fourier transforms.

$$u_n = \langle n|u\rangle = \langle n| \left( \sum_{k=0}^{N-1} |k\rangle\langle k| \right) |u\rangle = \sum_{k=0}^{N-1} \langle n|k\rangle F_k(u)$$

$$= \sum_{k=0}^{N-1} \frac{1}{\sqrt{N}} \exp(-i\frac{2\pi nk}{N}) F_k(u), \quad (\text{A5})$$

$$F_k(u) = \langle k|u\rangle = \langle k| \left( \sum_{n=0}^{N-1} |n\rangle\langle n| \right) |u\rangle$$

$$= \sum_{n=0}^{N-1} \langle k|n\rangle \langle n|u\rangle = \sum_{n=0}^{N-1} \frac{1}{\sqrt{N}} \exp(i\frac{2\pi nk}{N}) u_n \quad (\text{A6})$$

### 1. Functions of position and time

Suppose we have a function  $u$  = of the particle number  $n$  and time  $t$ , its value at a particle and time  $u_n(t)$ , are the components of the function  $u$  represented as the ket  $|u\rangle$  in the basis with elements  $|n, t\rangle$ , i.e.  $\langle n, t|u\rangle = u_n(t)$ . In principle,  $t$  is a continuous variable but, in practice, it is a discrete one obtaining by the sampling of numerical integration. So, if there are  $N_t$  time samples,  $t_l = l\Delta t$ , with  $l = 0 : N_t - 1$  and  $\Delta t$  the sampling interval. We change the basis notation to  $|n, l\rangle$ , with  $\langle n, t|u\rangle = u_n(t_l) = u_n(l\Delta t)$  and

$$|u\rangle = \sum_{n=1}^N \sum_{l=0}^{N_t-1} u_n(t_l) |n, l\rangle.$$

The basis  $|n, l\rangle$  is orthonormal, i.e.  $\langle n, l|n', l'\rangle = \delta_{n,n';l,l'}$ .

We assume that  $u_n(t_l+N_t) = u_n(t_l)$ , i.e., that  $u$  is time periodic with period  $T_f = N_t\Delta t$ . This is not a limitation as  $T_f$  is large enough that it has no consequences, similarly to Born-Von Karman boundary conditions in space.

Then, the alternative basis is given by the harmonic functions  $|k, s\rangle$ , with components:

$$\langle n, l|k, s\rangle = \frac{1}{\sqrt{NN_t}} \exp(-i[q_k n - \omega_s t_l]), \quad (\text{A7})$$

with period  $T_f$ , i.e.,  $\omega_s = \frac{2\pi s}{T_f} = \frac{2\pi s}{N_t\Delta t}$ , ( $s = 0 \dots N_t - 1$ ) with maximum frequency  $\frac{2\pi}{\Delta t}$ . Usually, frequencies are

shifted so as the zero frequency is the middle and then the maximum frequency is the Nyquist frequency  $2\pi/2\Delta t$ . Note that  $\Delta t$  determines the largest frequency, but the resolution is given by  $\frac{2\pi}{T_f}$ , that is, it depends on the final time.

The basis  $|k, s\rangle$  is also orthonormal as

$$\langle k, s | k', s' \rangle = \delta_{k,k';s,s'}. \quad (\text{A8})$$

Therefore,

$$\langle k, s | u \rangle = \sum_{k=0}^{N-1} \sum_{s=0}^{N_t-1} \langle k, s | n, l \rangle \langle n, l | u \rangle \quad (\text{A9})$$

$$= \frac{1}{\sqrt{NN_t}} \sum_{k=0}^{N-1} \sum_{s=0}^{N_t-1} \exp(-i[q_k n - \omega_s t_l]) u_n(t_l) \quad (\text{A10})$$

We can also obtain the expression of  $\frac{d^2}{dt^2}$  in  $k, w$  space. For that:

$$\frac{d^2}{dt^2} |k', s'\rangle = -\omega_{s'}^2 |k', s'\rangle \quad (\text{A11})$$

and then:

$$\langle k, s | \frac{d^2}{dt^2} |k', s'\rangle = -\omega_{s'}^2 \delta_{k,k';s,s'} \quad (\text{A12})$$

<sup>1</sup>M. Sato, B. E. Hubbard, and A. J. Sievers, “Colloquium: Nonlinear energy localization and its manipulation in micromechanical oscillator arrays,” *Rev. Mod. Phys.* **78**, 137–157 (2006).

<sup>2</sup>A. J. Sievers and S. Takeno, “Intrinsic localized modes in anharmonic crystals,” *Phys. Rev. Lett.* **61**, 970–973 (1988).

<sup>3</sup>J. B. Page, “Asymptotic solutions for localized vibrational modes in strongly anharmonic periodic systems,” *Phys. Rev. B* **41**, 7835–7838 (1990).

<sup>4</sup>S. Flach and A. Gorbach, “Discrete breathers in Fermi-Pasta-Ulam lattices,” *Chaos* **15**, 015112 (2005).

<sup>5</sup>Serge Aubry, “Breathers in nonlinear lattices: existence, linear stability and quantization,” *Physica D* **103**, 201–250 (1997).

<sup>6</sup>Masayuki Kimura and Takashi Hikihara, “Coupled cantilever array with tunable on-site nonlinearity and observation of localized oscillations,” *Phys. Lett. A* **373**, 1257–1260 (2009).

<sup>7</sup>M. Sato and A. J. Sievers, “Driven localized excitations in the acoustic spectrum of small nonlinear macroscopic and microscopic lattices,” *Phys. Rev. Lett.* **98**, 214101 (2007).

<sup>8</sup>Masayuki Kimura and Takashi Hikihara, “Capture and release of traveling intrinsic localized mode in coupled cantilever array,” *Chaos* **19**, 013138 (2009).

<sup>9</sup>Masayuki Kimura, Yasuo Matsushita, and Takashi Hikihara, “Parametric resonance of intrinsic localized modes in coupled cantilever arrays,” *Phys. Lett. A* **380**, 2823–2827 (2016).

<sup>10</sup>Christopher Chong, Andre Foehr, Efstrathios G. Charalampidis, Panayotis G. Kevrekidis, and Chiara Daraio, “Breathers and other time-periodic solutions in an array of cantilevers decorated with magnets,” *Math. Eng.* **1**, 489–507 (2019).

<sup>11</sup>Hirotaka Araki and Takashi Hikihara, “Shift manipulation of intrinsic localized mode in AC driven Klein Gordon lattice,” *Phys. Lett. A* **493**, 129270 (2024).

<sup>12</sup>Christopher Chong, Brian Kim, Evelyn Wallace, and Chiara Daraio, “Modulation instability and wavenumber bandgap breathers in a time layered phononic lattice,” *Phys. Rev. Res.* **6**, 023045 (2024).

<sup>13</sup>David J. Griffiths, *Introduction to Electrodynamics*, 5th ed. (Cambridge University Press, Cambridge, 2024).

<sup>14</sup>David J. Griffiths and Darrell F. Schroeter, *Introduction to Quantum Mechanics*, 3rd ed. (Cambridge University Press, Cambridge, 2018).

<sup>15</sup>Josh C. Slater, “Interaction of waves in crystals,” *Rev. Mod. Phys.* **30**, 197–222 (1958).

<sup>16</sup>E S Casseddy and A A Oliner, “Dispersion relations in time-space periodic media: Part i-Stable interactions,” *P. IEEE* **51**, 1342–1359 (1963).

<sup>17</sup>Juan F. R. Archilla, Yusuke Doi, and Masayuki Kimura, “Pterobreathers in a model for a layered crystal with realistic potentials: Exact moving breathers in a moving frame,” *Phys. Rev. E* **100**, 022206 (2019).

<sup>18</sup>S. Aubry, “Discrete breathers: Localization and transfer of energy in discrete Hamiltonian nonlinear systems,” *Physica D* **216**, 1–30 (2006).

<sup>19</sup>H. Marthinsen and B. Owren, “Geometric integration of non-autonomous linear hamiltonian problems,” *Adv. Comput. Math.* **42**, 313–332 (2016).

<sup>20</sup>Norman Y. Yao and Chetan Nayak, “Time crystals in periodically driven systems,” *Phys. Today* **71**, 40–47 (2018).

<sup>21</sup>Frank Wilczek, “Crystals in time,” *Sci. Am.* **321**, 28–35 (2019).

<sup>22</sup>A. J. Sievers and S. Takeno, “Intrinsic localized modes in anharmonic crystals,” *Phys. Rev. Lett.* **61**, 970–973 (1988).

<sup>23</sup>R. S. MacKay and S. Aubry, “Proof of existence of breathers for time-reversible or Hamiltonian networks of weakly coupled oscillators,” *Nonlinearity* **7**, 1623 (1994).

<sup>24</sup>J. L. Marín and S. Aubry, “Breathers in nonlinear lattices: Numerical calculation from the anticontinuous limit,” *Nonlinearity* **9**, 1501 (1996).

<sup>25</sup>S. Flach and A. V. Gorbach, “Discrete breathers. Advances in theory and applications,” *Phys. Rep.* **467**, 1–116 (2008).

<sup>26</sup>J. F. R. Archilla, J. Cuevas, B. Sánchez-Rey, and A. Alvarez, “Demonstration of the stability or instability of multibreathers at low coupling,” *Physica D* **180**, 235–255 (2003).

<sup>27</sup>Lingling Wu, Yong Wang, Kuochih Chuang, Fugen Wu, Qianxuan Wang, Weiqi Lin, and Hanqing Jiang, “A brief review of dynamic mechanical metamaterials for mechanical energy manipulation,” *Materials Today* **44**, 168–193 (2021).